UDK 621.762:621.762.5
Professional article/Strokovni članek

ISSN 1580-2949
MTAEC9, 48(2)305(2014)

INVESTIGATION OF INDUCTION AND CLASSICAL-SINTERING EFFECTS ON POWDER-METAL PARTS WITH THE FINITE-ELEMENT METHOD

PRIMERJAVA VPLIVA INDUKCIJSKEGA IN KONVENCIONALNEGA SINTRANJA NA DELCE KOVINSKEGA PRAHU Z UPORABO METODE KONČNIH ELEMENTOV

Göksan Akpınar, Can Çivi, Enver Atik

Celal Bayar University, Engineering Faculty, Mechanical Engineering Department, 45040 Manisa, Turkey
goksanakpinar105@hotmail.com

Prejem rokopisa – received: 2013-04-29; sprejem za objavo – accepted for publication: 2013-06-13

Induction sintering provides large time and energy savings because the components heat up rapidly and the sintering time is lower than in classical sintering in a furnace. Therefore, induction sintering is an important alternative to classical sintering. In this study, mechanical properties of induction-sintered Fe-based components including Cu and carbon (graphite) were compared with those sintered in a classical furnace. For this purpose, microstructure photographs of both samples were taken. A tensile analysis of the sintered powder-metal samples was carried out with the finite-element method, and the micro-stress values were found to change depending on the amount and distribution of the porosity.

Keywords: powder metallurgy, sintering, induction sintering, classical furnace, microstructure analysis, finite-element method

Indukcijsko sintranje omogoča velike prihranke pri času in energiji, saj se komponente ogrejejo hitro in je čas sintranja krajši, kot pri klasičnem sintranju v pečeh. Zato je indukcijsko sintranje pomembna alternativa klasičnemu sintranju. V tej študiji so bile primerjane mehanske lastnosti indukcijsko sintrane komponente z Fe-osnovo in dodatki Cu ter grafita s komponentami, sintranimi v klasičnih pečeh. V ta namen so bili napravljeni posnetki mikrostrukture obeh vzorcev. Izvršena je bila analiza nateznih preizkusov sintranih kovinskih vzorcev z metodo končnih elementov. Ugotovljeno je bilo, da so vrednosti mikronapetosti odvisne od količine in porazdelitve poroznosti.

Ključne besede: metalurgija prahov, sintranje, indukcijsko sintranje, klasična peč, analiza mikrostrukture, metoda končnih elementov

1 INTRODUCTION

Powders with different compositions are pressed and then sintered with the powder-metallurgy (P/M) method. Sintering is one of the most important issues of powder metallurgy because it causes a significant increase in the strength of the pressed powders. The sintering process is generally performed in sintering furnaces. It is done in a protective atmosphere of batch or continuous furnaces.[1] In addition, rapid sintering methods such as induction sintering, microwave sintering, plasma sintering, laser sintering and discharge sintering are important alternatives to conventional sintering methods.[2] Sintering and additional heat treatments of powder mixtures cause the microstructure to meet the performance requirements.[3]

Mixtures of elemental iron and graphite powders are commonly used for P/M applications. A small amount of copper powder is always added to further strengthen the sintered alloys owing to its relative ease of dissolving and diffusing in an iron matrix upon sintering.[4]

Almost all low-alloy steel powders contain copper. The mass fractions of copper varies between approximately 1 % and 8 % depending upon the desirability of end products. A small amount of copper is added to provide strength by age hardening, while the purpose of higher concentrations is to promote liquid-phase sintering causing a faster densification and homogenization.[5] An addition of carbon to iron powder increases the sintering kinetics as it dissolves into the iron lattice, changing the melting point, surface tension and viscosity of the iron melt formed. Small areas of martensite and tempered martensite are also formed. [6]

The most important feature of the induction-heating system is a rapid heating of the material because heating occurs directly on the metal parts. In general, induction sintering is used for surface heating of materials.[7] If the frequency increases, eddy currents will occur on the region close to the surface.[8] The heat transfer is 3.000 times better than in the other heating systems.[7] This allows a much faster completion of the warm-up process, reducing the time spent for this period and, thus, shortening the sintering time.

In addition, sintered ferrous P/M components have emerged as attractive candidates to replace wrought alloys in many applications due to their low cost, high performance and the ability to be processed to the near-net shape. Sintered materials are typically characterized by the residual porosity after sintering, which is quite detrimental to the mechanical properties of these materials.[9–17] The nature of the porosity is controlled with

several processing variables such as green density, sintering temperature and time, alloying additions, and the particle size of the initial powders.[10] In particular, the fraction, size, distribution and morphology of the porosity have a profound impact on mechanical behavior. Alloying elements such as copper, nickel and graphite affect the sintering parameters leading to the formation of a heterogeneous internal structure. Thus, the heterogeneous nature of the microstructures of P/M steels will certainly play a role in the onset and evolution of damage under an applied stress.[11–17] Under a monotonic tensile loading, the porosity reduces the effective load-bearing cross-sectional area acting as a stress-concentration site for the strain localization and damage, decreasing both strength and ductility.[11] Interconnected porosity causes an increase in the localization of the strain on the relatively smaller sintered regions between the particles, while isolated porosity results in a more homogeneous deformation. It is also not uncommon for the porosity distribution in a material to be inhomogeneous. In this case, the strain localization will take place at the "pore clusters". Thus, for a given amount of porosity, the interconnected porosity is more detrimental, reducing the macroscopic ductility to a greater extent than the isolated porosity.[17]

Porosity affects the mechanical properties of materials. Many studies have been conducted on this topic. N. Chawla and X. Deng[17] investigated the effects of mechanical properties, the shape and size factors of the porosity of sintered Fe–0.85Mo–Ni steels. They systematically examined the effect of porosity on the tensile and fatigue behaviors of the Fe–Mo–Ni steel. The steels of three densities were studied: 7.0 g/cm^3, 7.4 g/cm^3 and 7.5 g/cm^3. A quantitative analysis of the microstructure was performed to determine the pore-size distribution and the pore shape as functions of the sintered density. Holmes and Queeney[18] proposed that the relatively high stress concentration at pores, particularly the surface pores, is responsible for the localized slip leading to a crack initiation. Christian and German[19] showed that the fraction of porosity, pore size, pore shape and pore spacing are all important factors controlling the fatigue behavior of P/M materials. In general, more irregular pores exhibit a higher stress than perfectly round pores.[10] Polasik et al.[15] showed that small cracks nucleate from the pores during the fatigue and coalesce to form a larger crack leading to a fatigue fracture. Here, the heterogeneous nature of the microstructure played an important role by contributing to the crack tortuosity. Crack arrest and crack deflection were observed due to microstructural barriers such as particle boundaries, fine pearlite, and nickel-rich regions.[15]

In this study, the microstructures of classically sintered and induction-sintered metal-powder parts with a medium/low frequency (30 kHz) obtained with the experimental studies were compared. The effects of the sintering time on the mechanical properties were identified with image processing and the finite-element method. The micro-stresses around the internal spaces in the microstructures were investigated.

2 MATERIALS AND METHODS

In this study, the Högenas ASC 100.29 iron powder (2 % Cu, 0.5 % graphite and 1 % Zn Stereat lubricant by mass) was used. Powder-metal bushings were produced by Toz Metal Inc. with a dual-axis press under a 600 MPa pressure. The sieve analysis of the iron powder is shown in **Table 1.**[20] Induction and classical sintering mechanism are indicated in **Figure 1**. Powder-metal bushings with the dimensions of Φ16/14 mm × 36 mm are shown in **Figure 2**.

Table 1: Sieve analysis of the metal powder[20]
Tabela 1: Sejalna analiza kovinskega prahu[20]

Iron powder	Sieve analysis (%)			
ASC 100.29	< 45 μm	45–150 μm	150–180 μm	> 180 μm
	23	69	8	0

The powder-metal bushings were sintered in an environment atmosphere in an electric-resistance furnace

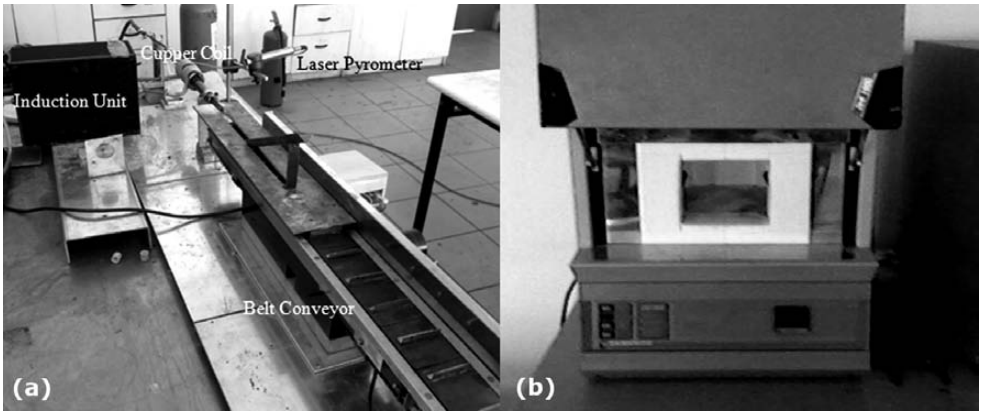

Figure 1: a) Induction-sintering mechanism, b) classical resistance furnace
Slika 1: a) Naprava za indukcijsko sintranje, b) klasična uporovna peč

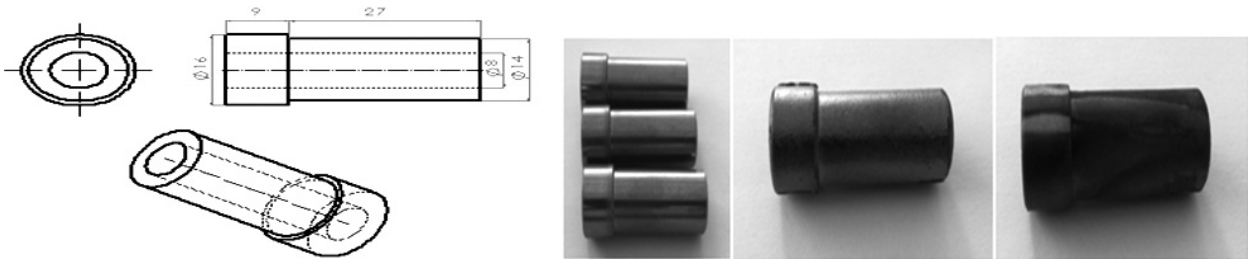

Figure 2: Sintered bushings
Slika 2: Sintrane puše

for 30 min at 1120 °C and they were also sintered by induction sintering for 8.4 min and 15 min at 1120 °C in the environment atmosphere. Induction sintering was carried out in a heat-resistant glass in a copper coil. The microstructural mechanical properties of these samples sintered for different periods and in different furnaces are compared with each other.

The induction sintering was carried out in a heat-resistant glass in a 36 mm diameter copper coil. The conveyor belt system is suitable for a mass production. The sintering temperature of 1120 °C was recorded on a pyrometer with laser and it was kept constant with the induction-mechanism unit. The sintered powder-metal bushings were cut and the microstructure images of the specimens were investigated using a Nikon Eclipse LV100 microscope. The cross-sections of the steel specimens were ground, polished and etched with a 2 % Nital solution (2 % HNO_3 and 98 % alcohol). The images of the polished surfaces of the cross-sections were taken.

The microstructures of the samples (40 μm) were processed by image processing. A tensile stress was applied to the samples with the finite-element method and the micro-stress values were obtained for the samples. The solution was made with an adoption of the mechanical properties of the steel containing 0.6 % graphite.

3 RESULTS

3.1 Microstructural analysis

A microstructural investigation was applied to the sintered bushings after polishing the surface with alumina and acid etching with a 3 % Nital solution. The microstructural photos are shown in **Figures 3** to **5**.

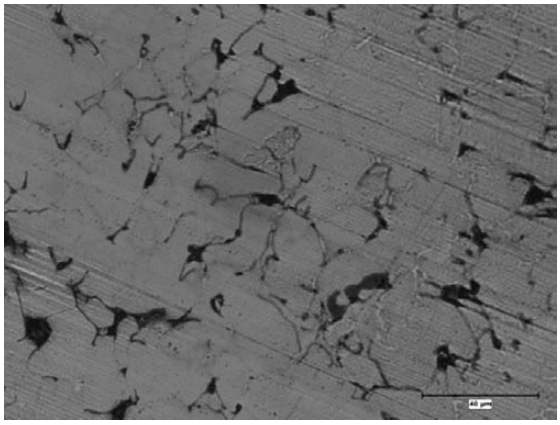

Figure 4: Microstructure of an induction-sintered powder-metal bushing (sintered at 1120 °C for 8.4 min), light microscope (LM), a 100-times magnification
Slika 4: Mikrostruktura indukcijsko sintrane puše iz kovinskega prahu (sintrano pri 1120 °C za 8,4 min), svetlobni mikroskop, povečava 100-krat

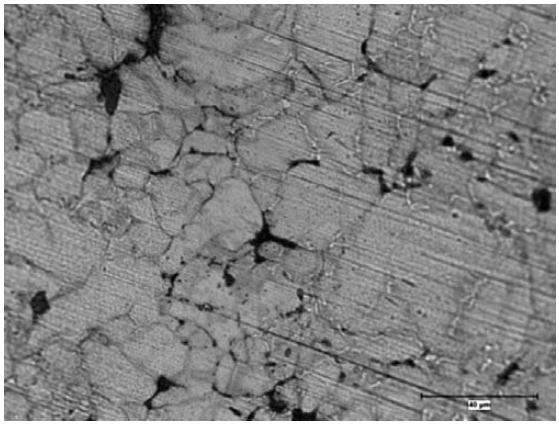

Figure 3: Microstructure of a classically sintered powder-metal bushing (1120 °C/30 min in the furnace), light microscope (LM), a 100-times magnification
Slika 3: Mikrostruktura klasično sintrane kovinske puše (1120 °C/30 min v peči), svetlobni mikroskop, povečava 100-krat

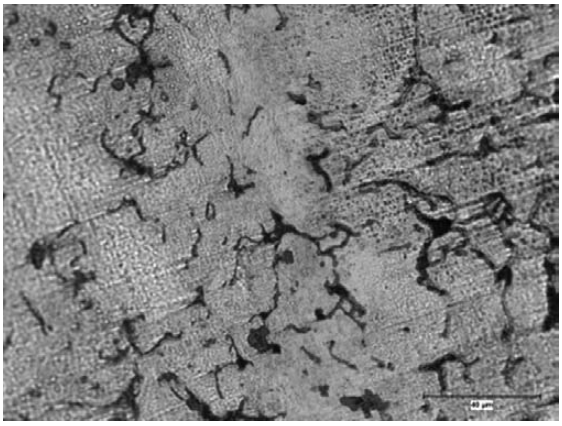

Figure 5: Microstructure of an induction-sintered powder-metal bushing (sintered at 1120 °C for 15 min), light microscope (LM), a 100-times magnification
Slika 5: Mikrostruktura indukcijsko sintrane kovinske puše (sintrano pri 1120 °C za 15 min), svetlobni mikroskop, povečava 100-krat

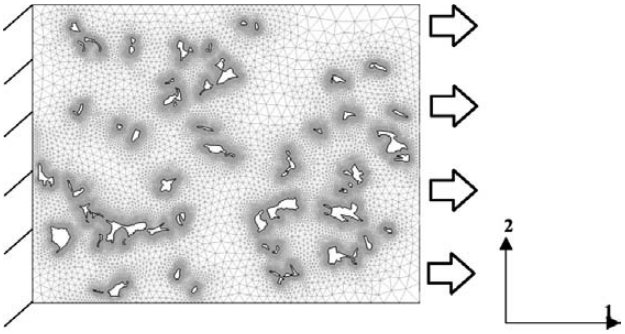

Figure 6: Finite-element boundary conditions of the real-microstructure image of a powder-metal part
Slika 6: Robni pogoji za analizo z metodo končnih elementov na realni mikrostrukturi sintranega kovinskega dela

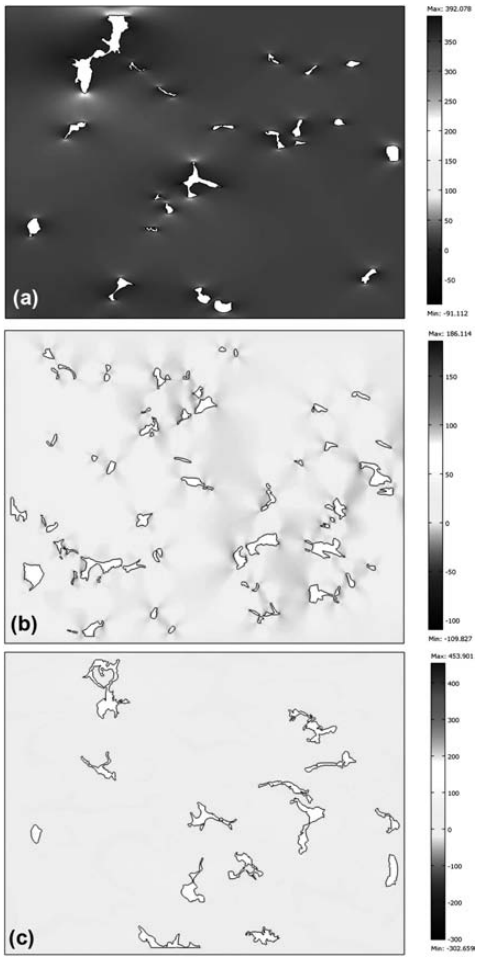

Figure 7: a) Microstructure of a powder-metal bushing classically sintered for 30 min in the furnace, a finite-element model of microstructure images with normal stress (MPa), b) microstructure of a powder-metal bushing induction sintered for 8.4 min, a finite-element model of microstructure images with normal stress, c) microstructure of a powder-metal bushing induction sintered for 15 min, a finite-element model of microstructure images with normal stress
Slika 7: a) Mikrostruktura klasično sintrane kovinske puše 30 min v peči; model mikrostrukture z metodo končnih elementov z normalno napetostjo (MPa), b) mikrostruktura indukcijsko sintrane kovinske puše (8,4 min); model mikrostrukture z metodo končnih elementov z normalno napetostjo, c) mikrostruktura indukcijsko sintrane kovinske puše (15 min); model mikrostrukture z metodo končnih elementov z normalno napetostjo

3.2 Image processing and FEM Analyses of microstructure pictures

The mechanical properties of the materials are shown in **Table 2**. The porosity values obtained from the image analysis of the samples are shown in **Table 3**. The maximum and minimum micro-stresses of the static tensile strength acting horizontally (1 direction) on the internal pores were found and compared with each other. The results of the study using the finite-element method are shown in **Figures 6** to **10**.

Table 2: Mechanical properties of the iron-based sintered material with 0.6 % graphite added and the loading conditions of the samples
Tabela 2: Mehanske lastnosti sintranega materiala z dodatkom 0,6 % grafita in razmere pri obremenitvi vzorcev

Poisson's ratio (an approximation)	Thermal-expansion coefficient (1/K)	F_x – Edge load, 1-direction (N/m²)
0.3	11.8 E–6	20 E6

4 DISCUSSION

It is well known that porosity decreases the Young's modulus of a material.[10] We use the approach of Ramakrishnan and Arunachalam (R–A)[21] to model the effect of the porosity on the Young's modulus. The Young's modulus of a material, E, with a given fraction of porosity, p, is given by:

$$E = E_0 \left[(1 - p)^2 / (1 + \kappa E_p)\right] \quad (1)$$

where E_0 is the Young's modulus of a fully dense steel (obtained by extrapolating the experimental data to the zero porosity, yielding a value of approximately 200 GPa), and κE is the constant in terms of the Poisson's ratio of a fully dense material, v_0:

$$\kappa E = 2 - 3v_0 \quad (2)$$

For a fully dense steel, the Poisson's ratio is approximately 0.3. This is supported by the analysis of Ramakrishnan and Arunachalam,[21] who compared the bulk modulus of porous materials with the spherical-versus-angular-pore geometry using FEM. An analytical solution was made to show that, depending on the density and porosity, the samples of the microstructures were

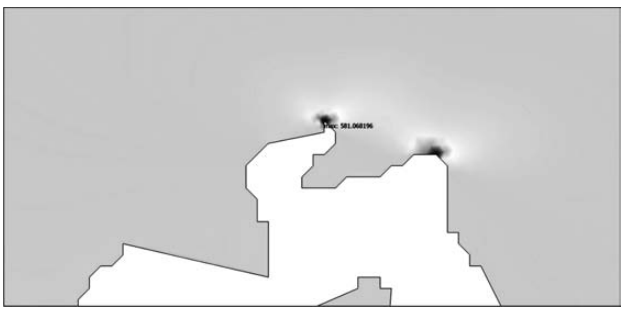

Figure 8: Induction-sintered sample 15 min, the maximum stress (MPa) in the area of the porosity of the microstructure
Slika 8: Indukcijsko sintran vzorec 15 min, največja napetost (MPa) na območju poroznosti v mikrostrukturi

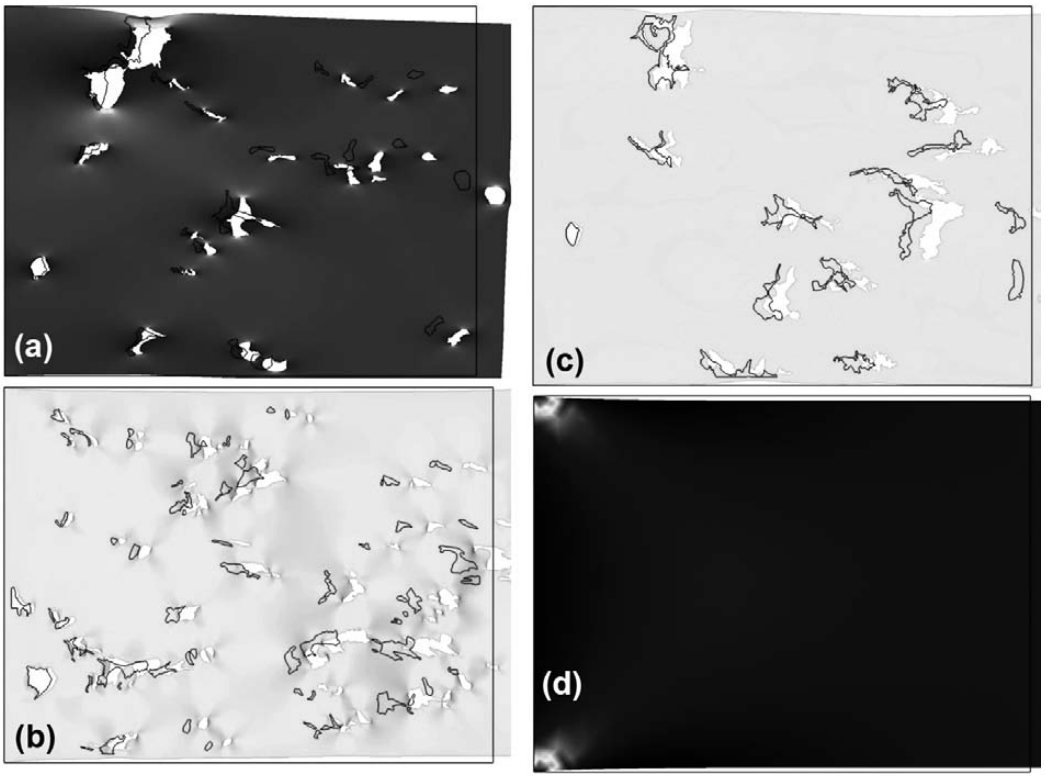

Figure 9: Finite-element investigation of the microstructures of the samples with both deformed and undeformed shapes: a) powder-metal bushing classically sintered for 30 min in the furnace, b) powder-metal bushing induction sintered for 8.4 min, c) powder-metal bushing induction sintered for 15 min, d) bulk material

Slika 9: Preiskava mikrostrukture z metodo končnih elementov vzorcev v deformiranem in nedeformiranem stanju: a) klasično sintrana kovinska puša (30 min v peči), b) indukcijsko sintrana kovinska puša (8,4 min), c) indukcija sintrana kovinska puša (15 min) in d) osnovni material

Table 3: Porosity, stresses and total-displacement values obtained from the image-processing analysis

Tabela 3: Poroznost, napetosti in skupen pomik, dobljeni iz analize slik

Samples	Porosity from image analysis (%)	Density (kg/m³)	Maximum stress around a pore (MPa)	Minimum stress around a pore (MPa)	Total displacement (μm)	Young's modulus (GPa)
Average of the samples induction sintered for 8.4 min	3.5411	7270	794.128	–234.780	2.31 E–2	185.684
Average of the samples induction sintered for 15 min	3.1846	7352	581.068	–473.677	3.186 E–2	187.077
Average of the samples classically sintered for 30 min	2.4004	7474	708.883	–228.570	2.774 E–2	190.177
Bulk sample	0	7860	34.171	17.967	1.691 E–2	200.000

affected by micro-stresses. The Young's modulus values of the samples are given in **Table 3**.

Although the finite-element analysis was used to study the mechanical behaviors of powder-metallurgy materials,[16,22–24] the pores are generally modeled as perfect spheres. But, at critical values of strain the imperfections cause localization of plastic flow.[24] In the R-A model a single spherical pore is surrounded by a spherical matrix shell, causing an intensification of the pressure on the pore surface due to the interaction of the pores in the material.[25] The material behavior is controlled by the microstructure of steel, in particular, the nature of the porosity.[17]

In this study we used two-dimensional microstructures as the basis for the finite-element simulations of the samples induction sintered for 8.4 minutes and 15 min, and the samples classically sintered for 30 min in a furnace. **Figure 6** shows the actual microstructure version of the uniaxial loading, boundary conditions and the mesh. A quadratic triangular mesh modeling was deemed appropriately. A finer mesh was used in the regions of pore clusters. In order to yield accurate simulation results, we used an entire picture of the microstructure simulation. The 2D analysis presented here shows the qualitative effects of the pore microstructure on the localized plastic strain and stress initiation around the pores. The porosity values of the samples, the maximum and minimum normal stresses, the Young's modulus, the total displacement, thermal-expansion coefficient values,

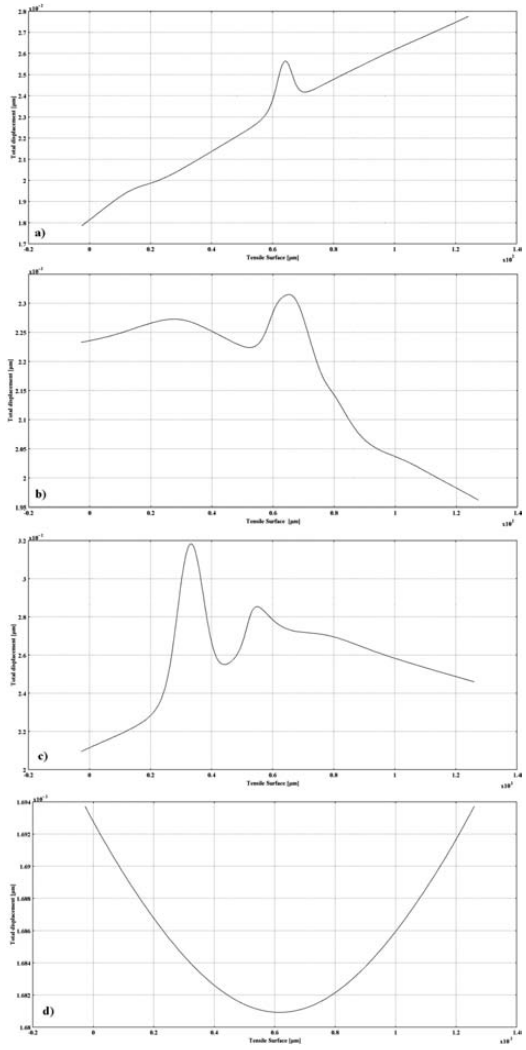

Figure 10: Total displacement curves of the tensile surfaces: a) powder-metal bushing classically sintered for 30 min in the furnace, b) powder-metal bushing induction sintered for 8.4 min, c) powder-metal bushing induction sintered for 15 min, d) bulk material

Slika 10: Skupni premik natezno obremenjene površine: a) klasično sintrana kovinska puša (30 min v peči), b) indukcijsko sintrana kovinska puša (8,4 min), c) indukcija sintrana kovinska puša (15 min) in d) osnovni material

the Poisson's ratio and the edge 1-direction loads are shown in **Tables 2** and **3**.

The normal stress around the pores, the total displacement, the deformed and undeformed shapes of the microstructures of the samples are shown in **Figures 7** and **9**. These figures show that the porosity was caused by an inhomogeneous deformation. The modeling also shows that the plastic-strain intensification begins at the tips of the irregular pores in the microstructure. This means that the more irregular the porosity, the more damage can be seen in the microstructure. For a regular deformation, as well as the porosity shape, the distribution of porosity in a structure is also important. Vedula and Heckel[9] investigated the mechanisms of a damage of flat and angular pores in a microstructure. They observed the forming of local shear bands at the ends of the pores, creating unstable tensions around the angular pores.

A mesh view and the finite-element boundary conditions of a real-microstructure image of a powder-metal part is shown in **Figure 6**. The solutions for each sample were compared by applying the same boundary conditions. Also, the local plastic strain acting around the micropores was found to be a result of the two-dimensional analysis. Each sample of the tensile surface is taken to have a value of $F_1 = 20$ N/m^2 for the stress-edge 1-direction load.

The stress equation of the modeling is as follows:[25]

$$F(\sigma_{ij} - \xi_{ij}) - h(\lambda h) = 0 \qquad (3)$$

where σ_{ij} is the symmetric stress index, ξ_{ij} is the first cycle of the yield surface, lh is the scalar function of the plastic strain and $h(\lambda$h) refers to the amount of expansion of the yield surface.

The stress concentrations at the tips of irregular pores in the microstructure are shown in **Figure 7**. Also, for the area around the pores of the sintered samples, the normal-stress FE-analysis results are given.

The maximum stress around the pores of the sample induction sintered for 8.4 min was 794.1 MPa. For the sample induction sintered for 15 min, a relatively lower value of 581.5 MPa for the maximum stress was obtained. On the basis of these results, it can be concluded that the maximum-stress value around the pores decreases with an increase in the density. As you can see in **Figure 8**, the maximum stress in the area of porosity depends not only on the density but also on the pore shape. The maximum stress for the microstructure of the sample induction sintered for 15 min is also shown in **Figure 8**. However, we have a difficulty here: although the sample induction sintered for 15 min showed the lowest tensile stress, the maximum stress value in the opposite direction is –473.7 MPa, which is higher than the other values. This result shows that the pore shape of a microstructure plays a key role in the micro-tensile stress.

The non-deformed and deformed shapes of the samples were analyzed. Despite having the lowest density, the induction-sintered sample 8.4 min showed a more uniform deformation than the other porosity samples. According to these results, smaller and regular pores contribute to a uniform deformation. When comparing the amounts of deformation in the porosity samples and the bulk sample, the porosity samples are found to be more deformed than the bulk sample. It can be said that the deformation amount of the samples depends on the pore shape as well as on the density.

The strain curves of the tensile surfaces of the samples are given in **Figure 10**. These strain curves appear to be quite different. The reasons for this difference are the rate, the shape and the pore density of the samples. As expected, the bulk sample has a symmetric deformation curve. When the inner tensile surface of the pores

increases, the surface-deformation-curve peak increases as well.

5 CONCLUSIONS

In this study, Fe-based powder-metal bushings were sintered with the classical-furnace and induction-sintering mechanisms. The microstructures of the classically sintered and induction sintered powder-metal bushings with a low to medium frequency (30 kHz) were compared. The effects of the sintering time on the mechanical properties were investigated with image processing and the finite-element method. The results show the following:

- The stresses that occurred around the pores in the microstructures of the samples were investigated numerically, showing how the stresses and displacement of the pores related to the sintering methods and parameter changes. Besides, it was also found that the mechanical properties of porous materials and the bulk material are quite different.
- Numerical results are shown in the **Table 3**. The maximum and minimum stresses for the samples classically sintered for 30 min are 708.9 MPa and –228.6 MPa, respectively. The maximum and minimum stresses for the sample induction sintered for 8.4 min are 794.1 MPa and –234.8 MPa, respectively. The maximum and minimum stresses for the samples induction sintered for 15 min are 581.5 MPa and –473.7 MPa, respectively, while the maximum and minimum stresses for the bulk samples are 34.2 MPa and 18 MPa, respectively.
- The pore sizes decrease with the increasing sintering time as illustrated in **Figure 7**. With the increasing induction-sintering time, large pores become relatively small, small pores disappear and the sintered density increases. On the other hand, when the induction-sintering time in the microstructures increases, lower and more homogenized tensile stresses occur around the pores.
- When looking at the values for the porosity obtained with the image analysis shown in **Table 3**, the minimum porosity value (2.4 %) is found for the samples classically sintered in the furnace for 30 min and, as expected, this porosity causes a smaller displacement than the other porosities. It is seen that the sample induction sintered for 8.4 min has a smaller displacement than the one induction sintered for 15 min. A more regular deformation is also shown in **Table 3** and **Figure 8**. According to this result, smaller and more regular pores of the sample induction sintered for 8.4 min are thought to cause a more regular deformation.
- The porosity samples were also compared to the bulk sample. It was seen that considerable internal stresses were formed around the pores of the porosity samples. This means that the material is exposed to tension, and the micro-stress concentrating around the pores can cause damage in a much shorter time. As a precaution, smaller and more regular pores should be formed in the microstructure and the microstructures of the materials should be concentrated.
- The microstructure-based FEM modeling showed that smaller, more regular and more clustered pores cause a more regular displacement and a reasonable micro-stress. So, the micro-stress and micro-strain depend on the pore shape and the loading condition as well as on the pore density.
- In our previous study, it was found that the strength values of the samples sintered with induction were increased by increasing the sintering time.[26] Due to more uniform and smaller pores in our current study, the micro-stress values of the sintered samples decreased. This also proves that the strength of the samples increases with a decrease in the micro-stress values.
- Another aim of this study was to investigate how the pores affect the micro-stress and micro-deformation. It was found that the strength of a porous material depends on the shape, the size and the density of the pores.

Acknowledgments

We would like to thank Toz Metal Inc. and Mr. Aytaç Ataş for providing the metal powder and pressing the powder-metal bushings.

6 REFERENCES

[1] R. M. German, Powder Metallurgy and Particulate Materials Processing, MPIF, New Jersey 2005

[2] E. Atik, U. Rye, Traditional and Fast Sintering Methods, CBU Soma Vocational School of Technical Sciences Journal, 1 (**2011**) 15

[3] K. S. Narasimhan, Sintering of powder mixtures and the growth of ferrous powder metallurgy, Materials Chemistry and Physics, 67 (**2001**) 1–3, 56–65

[4] W. F. Wang, Effect of alloying elements and processing factors on the microstructure and hardness of sintered and induction-hardened Fe–C–Cu alloys, Materials Science and Engineering, 402 (**2005**) 1–2, 92–97

[5] G. S. Upadhyaya, Effect of copper and VCN additions on sintering of low alloy steel, Materials & Design, 22 (**2001**) 5, 359–367

[6] A. Simchi, Effect of C and Cu addition on the densification and microstructure of iron powder in direct laser sintering process, Materials Letters, 62 (**2008**) 17–18, 2840–2843

[7] R. M. German, Sintering Theory and Practice, The Pennsylvania State University Park, Pennsylvania, A Wiley-Interscience Publication, Jon Wiley & Sons, Inc, USA 1996, 313–362, 373–400, 403–420

[8] A. H. Demırcı, Engineering Materials, Important Industrial Materials and Heat Treatment, Alfa Aktüel Press, 2004

[9] K. M. Vedula, R. W. Heckel, Modem Developments in Powder Metallurgy, Metal Powder Industries Federation, Princeton, NJ, 1981, 759

[10] A. Salak, Ferrous Powder Metallurgy, Cambridge International Science Publishing, Cambridge 1997

[11] A. Hadrboletz, B. Weiss, Int. Mater. Rev., 42 (**1997**), 1

[12] N. Chawla, S. Polasik, K. S. Narasimhan, M. Koopman, K. K. Chawla, Int. J. Powder Metall., 37 (**2001**), 49
[13] N. Chawla, T. F. Murphy, K. S. Narasimhan, M. Koopman, K. K. Chawla, Mater. Sci. Eng. A, 308 (**2001**), 180
[14] N. Chawla, D. Babic, J. J. Williams, S. J. Polasik, M. Marucci, K. S. Narasimhan, Advances in Powder Metallurgy and Particulate Materials, Metal Powder Industries Federation, 2002, 104
[15] S. J. Polasik, J. J. Williams, N. Chawla, Metall. Mater. Trans. A, 33 (**2002**), 73
[16] N. Chawla, B. Jester, D. T. Vonk, Mater. Sci. Eng. A, 346 (**2003**), 266
[17] N. Chawla, X. Deng, Microstructure and mechanical behavior of porous sintered steels, Materials Science and Engineering A, 390 (**2005**), 98–112
[18] J. Holmes, R. A. Queeney, Powder Metall., 28 (**1985**), 231
[19] K. D. Christian, R. M. German, Int. J. Powder Metall., 31 (**1995**), 51
[20] K. Widanka, Effect of Compacting Pressure on Interconnected Porosity in Iron PM Compacts, Powder Metallurgy Progress, 8 (**2008**) 1, 63–70
[21] N. Ramakrishnan, V. S. Arunachalam, J. Am. Ceram. Soc., 76 (**1993**), 2745
[22] R. Becker, J. Mech. Phys. Solids, 35 (**1987**), 577
[23] R. J. Bourcier, R. E. Smelser, O. Richmond, D. A. Koss, Inter. J. Fract., 24 (**1984**), 289
[24] R. J. Bourcier, D. A. Koss, R. E. Smelser, O. Richmond, Acta Metall., 34 (**1986**), 2443
[25] S. Suresh, Fatigue of Materials, second ed., Cambridge University Press, Cambridge 1998
[26] C. Çivi, E. Atik, AIP Conference Proceedings, 1476 (**2012**), 119–122